Neutron-proton pairing correlations and deformation for $N = Z$ nuclei in the pf shell within the deformed BCS and Hartree-Fock-Bogoliubov approach

Eunja Ha* and Myung-Ki Cheoun†
Department of Physics and Origin of Matter and Evolution of Galaxy (OMEG) Institute, Soongsil University, Seoul 156-743, Korea

H. Sagawa‡
RIKEN, Nishina Center for Accelerator-Based Science, Wako 351-0198, Japan and Center for Mathematics and Physics, University of Aizu, Aizu-Wakamatsu, Fukushima 965-8560, Japan

W. Y. So
Department of Radiological Science, Kangwon National University at Dogye, Samcheok 245-905, Korea

(Received 2 March 2018; revised manuscript received 12 May 2018; published 29 June 2018)

We investigated neutron-proton pairing correlations effects on the shell evolution of ground-state energies by the deformation for $N = Z$ nuclei in pf shell, such as ^{44}Ti, ^{48}Cr, ^{52}Fe, ^{64}Ge, ^{68}Se, ^{72}Kr, and ^{76}Sr. We started from a simple shell-filling model constructed by a deformed Woods-Saxon potential with β_2 deformation, and included pairing correlations in the residual interaction, which give rise to smearing of the Fermi surface revealing interesting evolution of the Fermi energy along the shell evolution. In this work, like-pairing and unlike-pairing correlations decomposed as isovector $T = 1$ and isoscalar $T = 0$ components are explicitly taken into account. Finally, we estimate ground-state energies comprising the mean-field energy, the pairing energy, and the self-energy due to the pairing correlations, in terms of the deformation. The enhanced $T = 0$ pairing interaction supports oblate deformations for ^{72}Kr and ^{68}Se, whose features are different from other pf-shell $N = Z$ nuclei considered in this work.

DOI: 10.1103/PhysRevC.97.064322

I. INTRODUCTION

Deformation in nuclei is one of the key ingredients of understanding the nuclear structure. In particular, weakly bound or neutron-rich (or neutron-deficient) nuclei show many interesting features by the deformation [1,2]. Deviation from the spherical shape usually needs nonspherical coordinate approaches. A typical approach for the deformation is to use the Nilsson basis [3] by using a deformed Woods-Saxon (WS) potential [4,5]. The single-particle spectrum obtained by the deformed WS potential is sensitive on deformation parameters, β_2 and β_4, defined as

$$R(\theta) = R_0[1 + \beta_2 Y_{20}(\theta) + \beta_4 Y_{40}(\theta)], \quad (1)$$

where the sharp-cut radius $R_0 = 1.2A^{1/3}$ fm [6], and Y_{20} and Y_{40} are spherical harmonics.

In general, shell evolution by the deformation becomes significant in neutron-rich nuclei, whose deformation can be confirmed by the $E2$ transition probability extracted from the experiments [7,8], and plays vital roles in understanding the β decays in nucleosynthesis. However, such features may also appear for neutron-deficient deformed nuclei, for example, in pf-shell $N = Z$ nuclei. In particular, according to theoretical calculations, ^{68}Se and ^{72}Kr are claimed to have oblate deformations while ^{44}Ti, ^{48}Cr, ^{52}Fe, ^{64}Ge, and ^{76}Sr have prolate (or spherical) deformations as tabulated in Table I.

In this paper, we discuss which deformation is the most stable by investigating the evolution of ground-state energies along with the deformation within a framework of the deformed Bardeen-Cooper-Schrieffer (DBCS) and deformed Hartree-Fock-Bogoliubov (DHFB). Specifically, ^{64}Ge is known to play a bottleneck role on the p or α processes [12,13]. Then the neutrino-proton (νp) process, $\bar{\nu}_e + p \rightarrow n + e^+$, produces many neutrons, which make it possible to escape the bottleneck by ^{64}Ge (n,p) ^{64}Ga (p,γ) ^{65}Ge reaction and subsequently bridge the waiting points. Therefore, the nuclear structure of ^{64}Ge and its β decay [14] become important for quantitative understanding ^{64}Ge (n,p) ^{64}Ga reaction.

On the other hand, pairing correlations, which comprise like-pairing [neutron-neutron (nn) and proton-proton (pp)] and unlike-pairing [neutron-proton (np)] correlations, are thought to play important roles in nuclear structure and relevant nuclear electromagnetic (EM) and weak transitions for $N = Z$ nuclei. In these nuclei, protons and neutrons occupy the same orbital and may have the maximum spatial overlap. The nn and pp pairings have isovector (IV) spin-singlet ($T = 1$, $J = 0$) mode, while the np-pairing correlations have isoscalar (IS) spin-triplet ($T = 0$, $J = 1$) as well as IV spin-singlet mode ($T = 1$, $J = 0$) [15–18]. Specifically, the $T = 0, J = 1$ mode is peculiar to the np-pairing correlations. Over the last few decades, there have been many discussions regarding the

*ejha@ssu.ac.kr
†Corresponding author: cheoun@ssu.ac.kr
‡sagawa@ribf.riken.jp

TABLE I. Deformation parameter β_2^{E2} from the experimental $E2$ transition data [7] and theoretical deformation parameters β_2 by relativistic mean-field (RMF) [9] and FRDM model [10] for $N = Z$ pf-shell nuclei. Empirical pairing gaps deduced from the five-point mass formula [11] are also tabulated.

Nucleus	β_2^{E2} [7]	$\beta_2^{\rm RMF}$ [9]	$\beta_2^{\rm FRDM}$ [10]	$\Delta_p^{\rm emp}$	$\Delta_n^{\rm emp}$	$\delta_{np}^{\rm emp}$
^{44}Ti	0.277 $(^{+12}_{-6})$	0.000	0.011	2.631	2.653	2.068
^{48}Cr	0.340 (19)	0.225	0.226	2.128	2.138	1.442
^{52}Fe	0.230 (14)	0.186	–0.011	1.991	2.007	1.122
^{64}Ge	0.259 $(^{+23}_{-17})$	0.217	0.207	1.807	2.141	1.435
^{68}Se	0.239 (16)	–0.285	0.233	1.909	2.174	1.522
^{72}Kr	0.330 (22)	–0.358	–0.366	2.001	1.985	1.353
^{76}Sr	0.443 $(^{+31}_{-25})$	0.410	0.402	1.626	1.657	0.715

np-pairing correlations, in particular, the IS and IV components and their competition and coexistence in some specific nuclear models [19–22]. Most studies focused on the $N = Z$ nuclei because the np pairing is expected to be larger than other $N \neq Z$ nuclei. However, as shown in a recent work [23], the nuclear structure of the $N \simeq Z$ nuclei may also be affected by the np-pairing correlations. For example, Ref. [23] found the mixing phase of the IS and IV condensation for nuclei with $60 < N < 70$ and $57 < Z < 64$.

Recently, more interesting experimental data are reported, which show the IV quenching in the $M1$ spin transition data for the $N = Z$ nuclei in sd shell [24]. It was suggested that the $T = 0$ pairing enhanced by the tensor force well known in the deuteron structure may become more significant even inside nuclei [25,26], which may lead to the IS condensation in nuclear symmetric matter. Since then there appeared many theoretical discussions about the quenching of the spin transitions related to the neutron-proton pairing [27–29]. Detailed reports about the present status and recent progress regarding the np-pairing correlations in the nuclear structure can be found at Refs. [30,31].

The importance of the np pairing was also discussed in our early papers for double-β-decay transitions by using a realistic two-body interaction given by the Brueckner G matrix based on the CD Bonn potential [11,32,33]. However, they were performed in a spherical QRPA, which did not include the deformation explicitly and the IS np pairing was taken into account by renormalizing the IV np-pairing component.

The aim of the present work is to study whether we can understand the nuclear shape evolution of pf-shell nuclei in the DBCS and/or DHFB approaches by including all kinds of pairing correlations with the quenching phenomena. Specifically, if we note that the isospin singlet condensation may be formed in the sd-shell nuclei [34], it would be quite interesting if the IS condensation may also be formed in the pf-shell nuclei. In that context, this work is a general extension of the previous works [34–37].

II. FORMALISM FOR DEFORMED BCS AND DEFORMED HFB

Since the theoretical framework for the DBCS approach had already been detailed in our previous papers [34,35], here only the basic formula is briefly stated. We start from the following nuclear Hamiltonian:

$$\begin{aligned} H &= H_0 + H_{\rm int}, \\ H_0 &= \sum_{\rho_\alpha \alpha\alpha'} \epsilon_{\rho_\alpha \alpha\alpha'} c^\dagger_{\rho_\alpha \alpha\alpha'} c_{\rho_\alpha \alpha\alpha'} \quad , \\ H_{\rm int} &= \sum_{\rho_\alpha\rho_\beta\rho_\gamma\rho_\delta,\alpha\beta\gamma\delta,\alpha'\beta'\gamma'\delta'} V_{\rho_\alpha\alpha\alpha'\rho_\beta\beta\beta'\rho_\gamma\gamma\gamma'\rho_\delta\delta\delta'} \\ &\quad \times c^\dagger_{\rho_\alpha\alpha\alpha'} c^\dagger_{\rho_\beta\beta\beta'} c_{\rho_\delta\delta\delta'} c_{\rho_\gamma\gamma\gamma'}, \end{aligned} \tag{2}$$

where greek letters denote proton or neutron single-particle states with a projection Ω of a total angular momentum on a nuclear symmetry axis. $\rho_\alpha (\rho_\alpha = \pm 1)$ denotes a sign of the total angular momentum projection of a state α. Isospin of the particle is denoted by greek letter with prime. The operator $c^\dagger_{\rho_\alpha\alpha\alpha'}$ ($c_{\rho_\alpha\alpha\alpha'}$) in Eq. (2) stands for a usual creation (destruction) operator of the real particle in the state of $\alpha\rho_\alpha$. The Hamiltonian, represented by real particles in Eq. (2), was then transformed to a quasiparticle representation by the following DHFB transformation:

$$\begin{aligned} a^\dagger_{\rho_\alpha\alpha\alpha''} &= \sum_{\rho_\beta\beta\beta'} \left(u_{\alpha\alpha''\beta\beta'} c^\dagger_{\rho_\beta\beta\beta'} + v_{\alpha\alpha''\beta\beta'} c_{\rho_\beta\bar\beta\beta'} \right), a_{\rho_\alpha\bar\alpha\alpha''} \\ &= \sum_{\rho_\beta\beta\beta'} \left(u_{\bar\alpha\alpha''\bar\beta\beta'} c_{\rho_\beta\bar\beta\beta'} - v_{\bar\alpha\alpha''\bar\beta\beta'} c^\dagger_{\rho_\beta\beta\beta'} \right). \end{aligned} \tag{3}$$

Since our formalism is intended to include the np-pairing correlations, we denote the isospin of quasiparticle as α'' or $\beta'' = 1$ or 2. We assume the time-reversal symmetry, which means $u_{\alpha\alpha''\beta\beta'} = u^*_{\bar\beta\alpha''\bar\alpha\beta'}$ and $v_{\alpha\alpha''\beta\beta'} = -v^*_{\bar\beta\alpha''\bar\alpha\beta'}$. In the DHFB, the quasiparticle comprises particle and hole properties located in different deformed states, α and β.

On the other hand, the DBCS transformation for each α state is usually given as

$$\begin{pmatrix} a^\dagger_1 \\ a^\dagger_2 \\ a_{\bar 1} \\ a_{\bar 2} \end{pmatrix}_\alpha = \begin{pmatrix} u_{1p} & u_{1n} & v_{1p} & v_{1n} \\ u_{2p} & u_{2n} & v_{2p} & v_{2n} \\ -v_{1p} & -v_{1n} & u_{1p} & u_{1n} \\ -v_{2p} & -v_{2n} & u_{2p} & u_{2n} \end{pmatrix}_\alpha \begin{pmatrix} c^\dagger_p \\ c^\dagger_n \\ c_{\bar p} \\ c_{\bar n} \end{pmatrix}_\alpha , \tag{4}$$

where the u and v coefficients are calculated by the following DBCS equation:

$$\begin{aligned} &\begin{pmatrix} \epsilon_p - \lambda_p & 0 & \Delta_{p\bar p} & \Delta_{p\bar n} \\ 0 & \epsilon_n - \lambda_n & \Delta_{n\bar p} & \Delta_{n\bar n} \\ \Delta_{p\bar p} & \Delta_{p\bar n} & -\epsilon_p + \lambda_p & 0 \\ \Delta_{n\bar p} & \Delta_{n\bar n} & 0 & -\epsilon_n + \lambda_n \end{pmatrix}_\alpha \begin{pmatrix} u_{\alpha''p} \\ u_{\alpha''n} \\ v_{\alpha''p} \\ v_{\alpha''n} \end{pmatrix}_\alpha \\ &= E_{\alpha\alpha''} \begin{pmatrix} u_{\alpha''p} \\ u_{\alpha''n} \\ v_{\alpha''p} \\ v_{\alpha''n} \end{pmatrix}_\alpha . \end{aligned} \tag{5}$$

Here $E_{\alpha\alpha''}$ is the energy of the quasiparticle with isospin quantum number α'' in a α state. We include $n\bar p$ and $p\bar n$ pairings in addition to the like-pairing ($p\bar p$ and $n\bar n$) correlations. However, the np and $\bar n\bar p$ pairings in the same orbital (e.g., $|np, T = 0\rangle$ and $|\bar n\bar p, T = 0\rangle$) are not explicitly included, but implicitly taken into account by Eqs. (22)– (23) in Ref. [34].

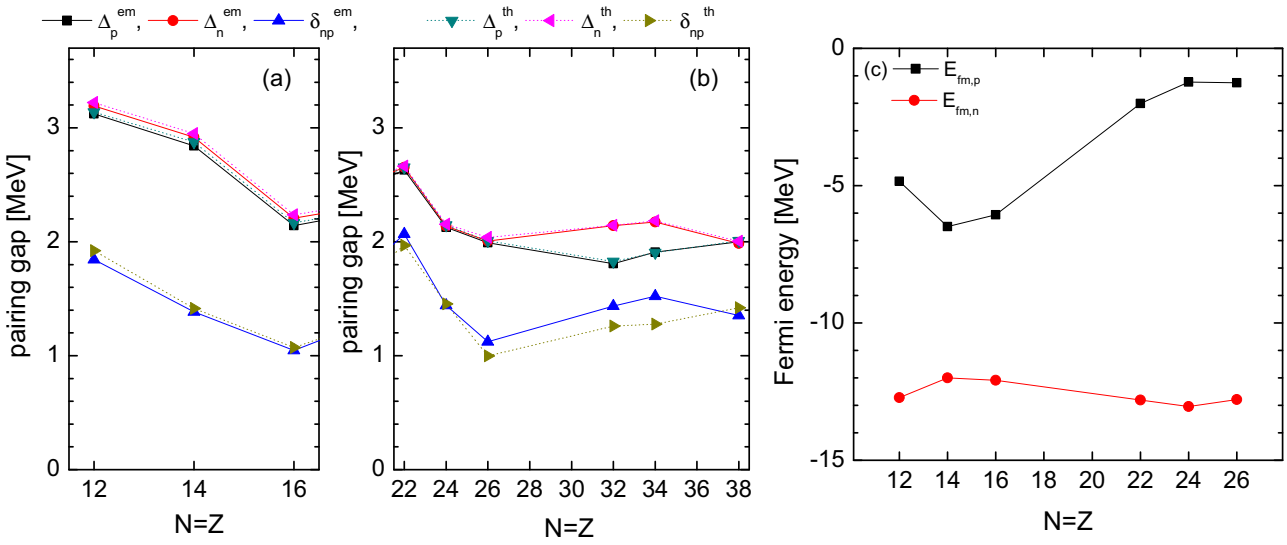

FIG. 1. Empirical ($\Delta^{\rm em}_{p,n}$ and $\delta^{\rm em}_{np}$) and theoretical ($\Delta^{\rm th}_{p,n}$ and $\delta^{\rm th}_{np}$) pairing gaps in (a) and (b), and Fermi energy evolution of protons and neutrons in (c) for sd and pf shell $N = Z$ nuclei.

In the DBCS, we do not allow pairings of the different deformed single-particle states (SPSs), α and β. However, in the present approach, a quasiparticle state is mixed with different spherical SPSs because each deformed state (basis) is represented by a linear combination of the spherical state (basis) (see Fig. 1 in Ref. [35]). This feature is one of additional merits due to the inclusion of deformation in the BCS approach, i.e., the DBCS approach. With the np pairing in the deformed basis it leads to a simple HFB-type transformation in the spherical basis [17].

The pairing potentials in the DBCS Eq. (5) were calculated in the deformed basis by using G matrix calculated from the realistic Bonn CD potential for nucleon-nucleon (N-N) interaction. At this step, we also tested the JK couplings between different deformed SPSs treated in the DHFB transformation in Eq. (3). For this end, the pairing potentials in Eq. (5) are extended to include the pairing between different γ and δ states as follows:

$$\Delta_{p\bar{p}_\alpha} = \Delta_{\alpha p\bar{\alpha}p} = -\sum_{J,c,d} g_{\rm pp} F^{J0}_{\alpha a\bar{\alpha}a} F^{J0}_{\gamma c\bar{\delta}c} G(aacd,J,T=1) \times \left(u^*_{1p_c} v_{1p_d} + u^*_{2p_c} v_{2p_d}\right), \quad (6)$$

$$\Delta_{p\bar{n}_\alpha} = \Delta_{\alpha p\bar{\alpha}n} = -\sum_{J,c,d} g_{\rm np} F^{J0}_{\alpha a\bar{\alpha}a} F^{J0}_{\gamma c\bar{\delta}c} \big[G(aacd,J,T=1) \times Re\left(u^*_{1n_c} v_{1p_d} + u^*_{2n_c} v_{2p_d}\right) + iG(aacd,J,T=0) \times Im\left(u^*_{1n_c} v_{1p_d} + u^*_{2n_c} v_{2p_d}\right)\big], \quad (7)$$

where $F^{JK}_{\alpha a\bar{\alpha}a} = B^\alpha_a B^\alpha_a (-1)^{j_a-\Omega_\alpha} C^{JK}_{j_a\Omega_\alpha j_a-\Omega_\alpha} (K = \Omega_\alpha - \Omega_\alpha)$ was introduced to represent the G matrix in the deformed basis with the expansion coefficient B_α [35]

$$B^\alpha_a = \sum_{Nn_z\Sigma} C^{j\Omega_\alpha}_{l\Lambda\frac{1}{2}\Sigma} A^{N_0 l}_{Nn_z\Lambda} b_{Nn_z\Sigma}, A^{N_0 l n_r}_{Nn_z\Lambda} = \langle N_0 l\Lambda | Nn_z\Lambda\rangle. \quad (8)$$

Here K is a projection number of the total angular momentum J onto the z axis, and selected as $K = 0$ at the DBCS stage. $G(aacd,J,T)$ matrix represents two-body scattering matrix calculated in the spherical basis. In the present work, we have included all possible J values in Eqs. (6) and (7), which have the $K = 0$ projection. $\Delta_{\alpha n\bar{\alpha}n}$ is the similar to Eq. (6) where n was replaced by p. Hereafter, we call these calculations as DHFB approach because this may include the effect by the DHFB transformation in Eq. (3).

In order to renormalize the G matrix, strength parameters, $g_{\rm pp}$, $g_{\rm nn}$, and $g_{\rm np}$ were multiplied to the G matrix [11] by adjusting the pairing potentials, $\Delta_{p\bar{p}}$ and $\Delta_{n\bar{n}}$, of the lowest state in Eq. (6) to empirical pairing gaps, $\Delta^{\rm emp}_p$ and $\Delta^{\rm emp}_n$. The empirical pairing gaps of protons and neutrons were evaluated by a symmetric five mass-term formula for neighboring nuclei in Ref. [35].

For the np pairing, we assume that the ground state of odd-odd nuclei has one unpaired proton and neutron with energies close to the Fermi surface and the attractive short-range interaction between them is to be the origin of the np-pairing interaction [11,18]. Therefore masses of the odd-odd nuclei are treated as a sum of even-even mass and the like-pairing gaps subtracted by the attractive residual np interaction energy, namely, $M(Z,N)_{\rm odd-odd} = M(Z,N)_{\rm even-even} + \Delta^{\rm emp}_p + \Delta^{\rm emp}_n - \delta^{\rm emp}_{np}$. Then the np-pairing gap was deduced as follows:

$$\delta^{\rm emp}_{np} = \pm\tfrac{1}{4}\{2[M(Z,N+1) + M(Z,N-1) + M(Z-1,N) + M(Z+1,N)] - [M(Z+1,N+1) + M(Z-1,N+1) + M(Z-1,N-1) + M(Z+1,N-1)] - 4M(Z,N)\}, \quad (9)$$

where the signs in the + (–) stand for even (odd) mass nuclei. Regarding the masses in Eq. (9), we used available empirical masses. By following the above argument, our theoretical np

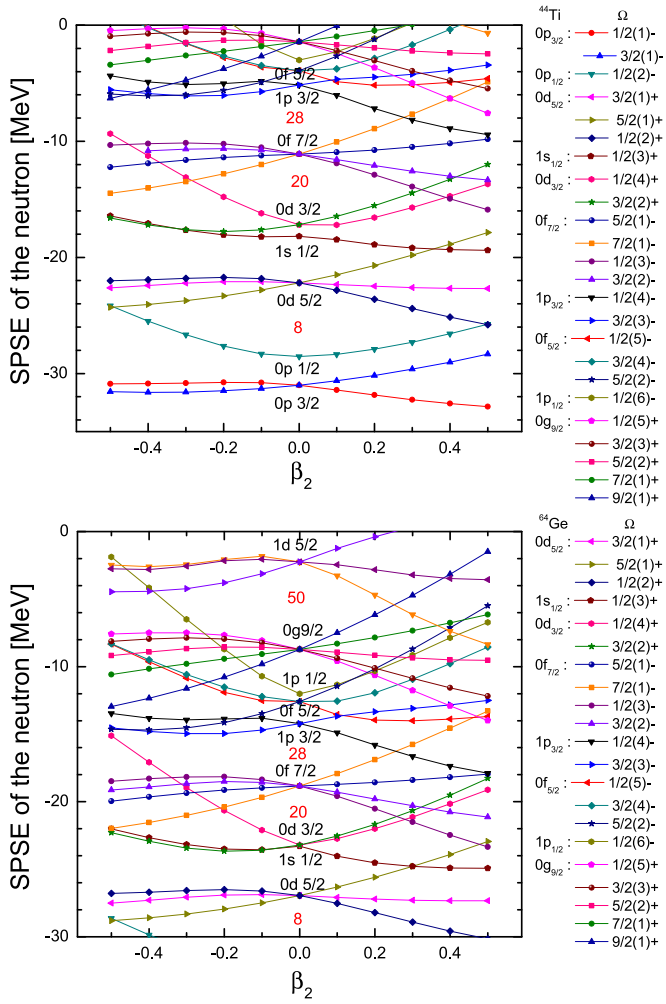

FIG. 2. Shell evolutions of single-particle states (SPSs) by the deformation for ^{44}Ti and ^{64}Ge. They are calculated by using a deformed Woods-Saxon potential with the optimal parameter set in Ref. [4].

pairing gaps were calculated as

$$\delta_{np}^{\text{th.}} = -\left[\left(H_{gs}^{12} + E_1 + E_2\right) - \left(H_{gs}^{np} + E_p + E_n\right)\right]. \quad (10)$$

Here $H_{gs}^{12}(H_{gs}^{np})$ is a total DBCS ground-state energy with (without) np pairing and $E_1 + E_2(E_p + E_n)$ is a sum of the lowest two quasiparticle energies with (without) np-pairing potential Δ_{np} in Eq. (5). For quantitative understanding of the np pairing as well as the like-pairing gap, we present empirical and theoretical pairing gaps in Fig. 1 with the Fermi energies calculated by the DBCS. The δ_{np} results for pf-shell nuclei in Fig. 1(b) are shown to be comparable to those for sd-shell nuclei in Fig. 1(a), while the like pairings become smaller with the increase of mass number.

Experimental masses used in Eq. (9) include all possible correlations beside the pairing correlations. It means that the present theoretical DBCS (or DHFB) approach for the pairing gaps used in this paper should be an approximation to the empirical gap. More refined approaches, for example, the (isospin) generalized BCS [17,19], which explicitly includes $|np\rangle$ and $|\bar{n}\bar{p}\rangle$ pairing as well as $|n\bar{p}\rangle$ and $|p\bar{n}\rangle$ pairing considered in this work are further desirable for deducing the empirical pairing gaps in a microscopic way. Here, we take a simple approach for the $\bar{n}\bar{p}$ and np pairing, for which we multiply a weight factor 2.0 for the $T = 0$ np pairing as discussed in our previous paper [34]. Also, for more exact treating the particle numbers in the DBCS or DHFB theory, one needs the Lipkin-Nogami method [38] and/or the projected BCS approach [39–42].

III. RESULTS AND DISCUSSIONS

This study exploited the cylindrical Woods-Saxon potential with the optimal parameter set reported by Cwiok *et al.* [4]. Other parameter sets show almost same results, at least, for the nuclei considered in this work [43]. The particle model space for all the nuclei was exploited up to $N = 5\hbar\omega$ for a deformed basis and up to $N = 10\hbar\omega$ for a spherical basis.

Evolutions of single-particle states (SPSs) by the deformation parameter β_2 are shown for ^{44}Ti and ^{64}Ge in Fig. 2. In a viewpoint of a simple shell-filling model, which distributes all particles up to the outermost shell by allocating two particles in each deformed SPS state, the shell gaps from the outermost shell are relatively small, less than 2 MeV, regardless of the deformation. It means that particles are easily jumped to the next shell, which makes more or less correlations and excitations. One point to notice is the shell evolution of the $1/2_4^+$ state (pink hexagons) in $0d_{3/2}$ shell, which is bounded stronger at $\beta_2 = 0$ rather than the prolate and oblate regions. But the $7/2_1^-$ state (orange squares) in $0f_{7/2}$ shell becomes looser with the prolate deformation while the $1/2_4^-$ state (black inverted triangles) in $1p_{3/2}$ shell is more bounded with the prolate deformation. Another point to notice is that the $N = 28$ magic shell is still valid number in whole deformation region except $\beta_2 \geqslant 0.3$ region and $N(= Z) = 34$ and 36 shells show relatively large energy gaps along the deformation, apart from $-0.25 < \beta_2 < 0$ region.

Usually the $T = 0$ pairing was not strong enough to manifest itself in the pairing energy [18,35]. However, recent $M1$ spin data [24] report that the IV spin transitions show more quenching than the IS ones and the IS $T = 0$ pairing interaction is pointed out to induce partially this quenching effect.

However, this data showing the IV spin quenching is limited to the $M1$ spin transition for sd-shell nuclei. In this work, we test the possibility of the IV quenching (or IS condensation) in pf-shell nuclei in the following. One more point to be noticed in the present scheme is that we did not explicitly include the np and $\bar{n}\bar{p}$ pairings. Therefore, in the third approach, we take into account the enhanced IS pairing interaction by multiplying a factor 1.5 to the corresponding matrix elements by following the results in Ref. [29]. We also effectively include the other $T = 0$ contribution due to the np and $\bar{n}\bar{p}$ pairings by multiplying a factor 2 to the $T = 0$ pairing by the $n\bar{p}$ and $p\bar{n}$ correlations. Therefore, the enhanced factor becomes three, whose detailed argument can be found at Ref. [34].

First, we examine the DHFB approach. In Fig. 3, we show the results of DBCS and DHFB calculations; Fig. 3(a) with $pp + nn$ pairings; Fig. 3(b), $pp + nn + np$ pairings; and Fig. 3(c) $pp + nn + np$ pairings with the enhanced $T = 0$ channel. In Fig. 3(a), the two results are almost identical,

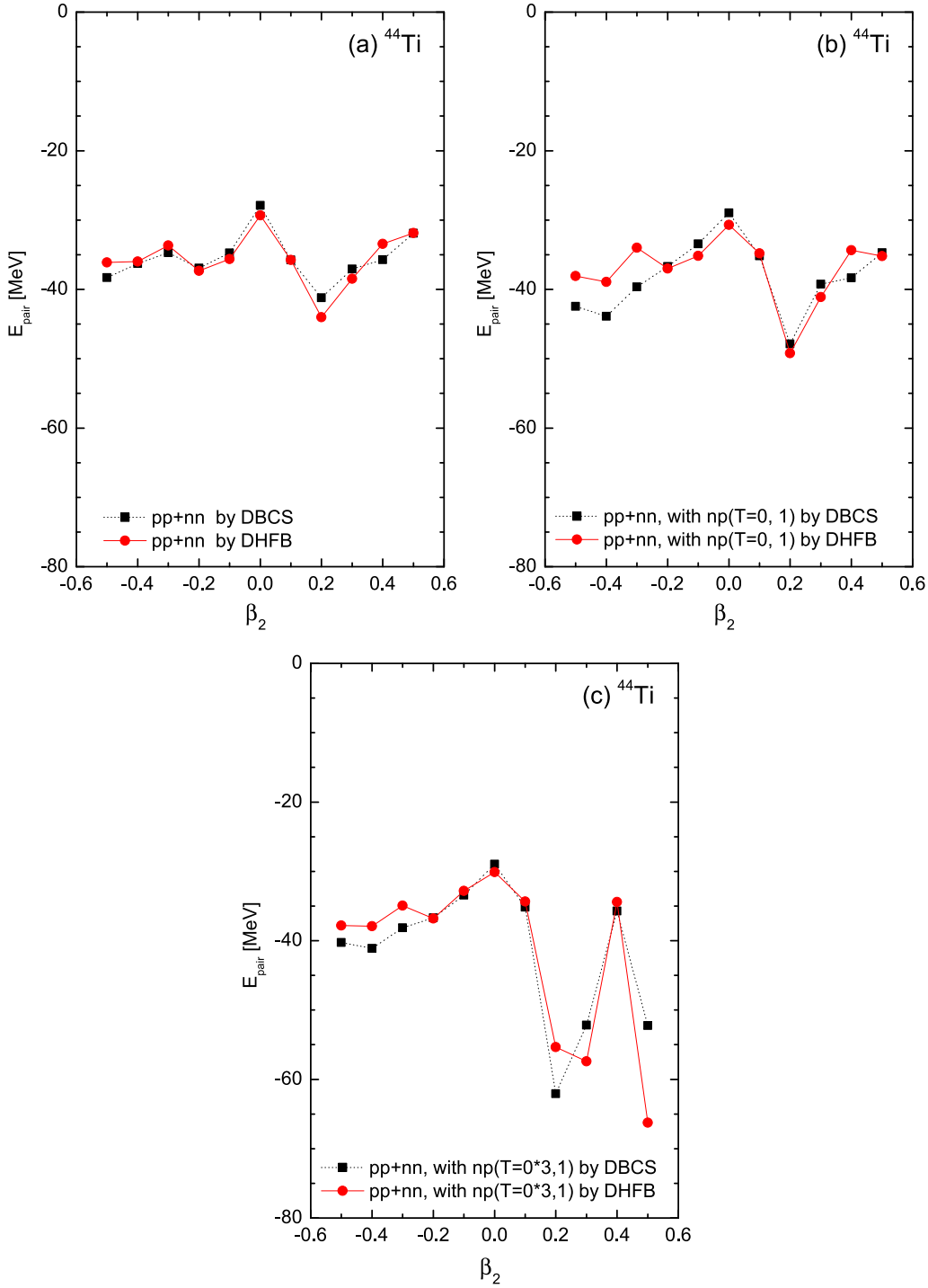

FIG. 3. Pairing correlation energies by DBCS and DHFB approximations as a function of quadrupole deformation parameter β_2. The pairing energies are estimated by three different cases, (a) without and (b) with the np pairing, and (c) with the three times enhanced $T = 0$ pairing.

while the np pairing in Fig. 3(b) gives rise to some differences between two results in oblate and prolate sides $|\beta_2| > 0.2$. In the case of the enhanced $T = 0$ pairing, one can also see some differences in both oblate and prolate sides. However, since these differences do not affect much the shell evolution by the deformation, we refer only the results of DBCS hereafter.

In the following (Figs. 4–12), we present our numerical results regarding total ground-state energies for ^{44}Ti, ^{48}Cr, ^{52}Fe, ^{64}Ge, ^{68}Se, ^{72}Kr, and ^{76}Sr, in terms of the deformation parameter β_2. Figures 4(a)–12(a) show ground-state energies (GSEs) by the simple shell-filling model, which means the occupation probability $v_a^2 = 1$ or 0 by no smearing. They are calculated with respect to the Fermi energy located in the outermost shell. Different evolutions of GSEs by the deformation can be easily understood by the shell evolution of SPSs in Fig. 2. A typical feature in the GSE evolution of these

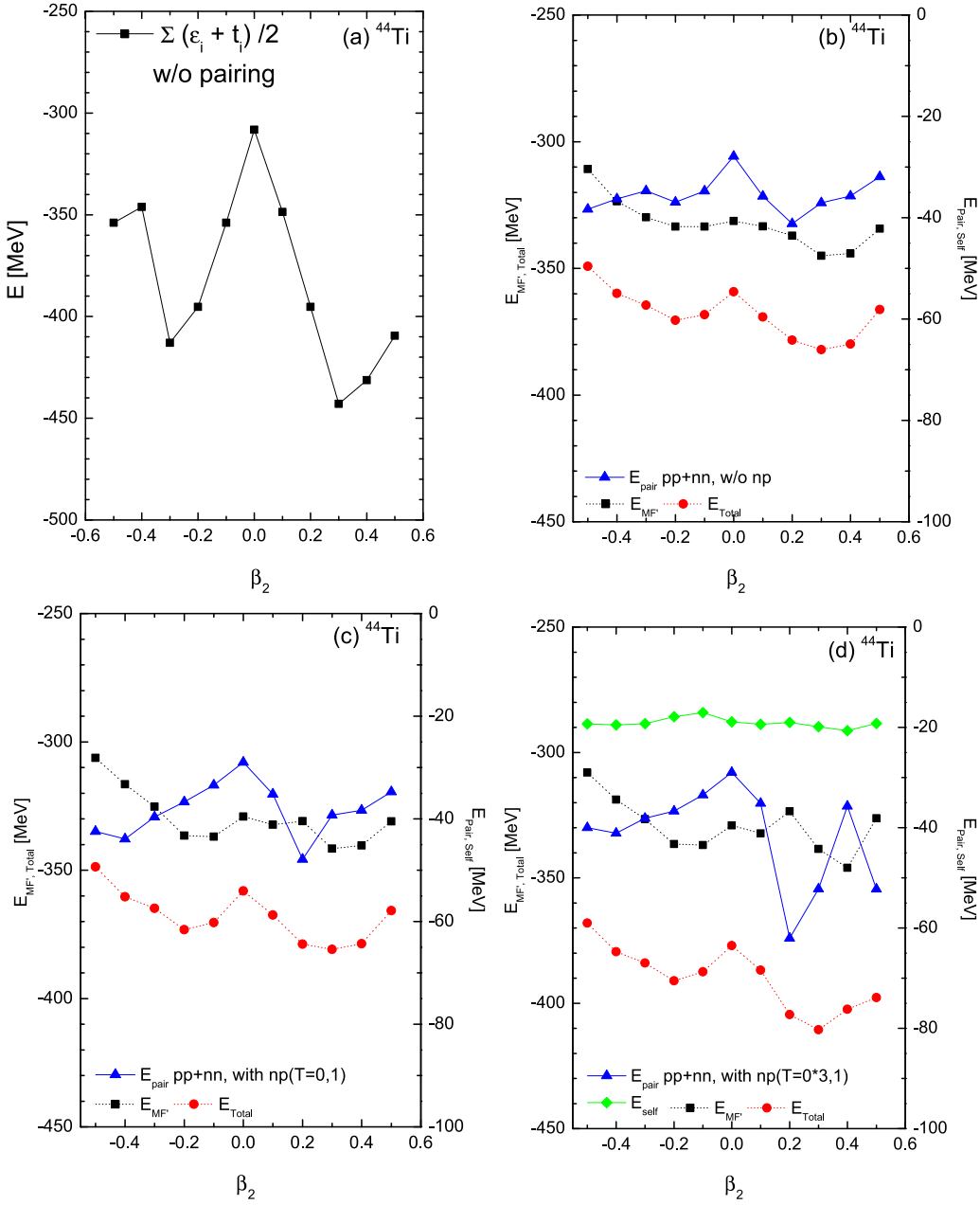

FIG. 4. Ground-state energy (GSE) for ^{44}Ti by the DBCS model based on a deformed Woods-Saxon potential [4]. Energies are estimated from the Fermi energy surface calculated by the DBCS. $E_{\mathrm{MF'}}$ is the mean-field energy with respect to the Fermi energy, which is different from the GSE in (a) because the Fermi energy is changed by the DBCS approach owing to the pairing interactions. E_{pair} is the pairing energy indicated in the right axis label. The pairing energies are estimated by three different cases, (b) without and (c) with the np pairing and (d) with the three times enhanced $T = 0$ pairing. (d) includes the self-energy due to the pairing interactions denoted as (green) diamond.

nuclei is a double valley. For example, for ^{44}Ti, left downhill in the oblate shape comes mainly from the evolution of the $1/2^+_4$ state in $0d_{3/2}$ shell. The uphill part in the prolate region results from the $7/2^-_1$ state in $0f_{7/2}$ shell, but the gradient becomes smaller than the oblate region by the downhill of the $1/2^-_4$ state in $1p_{3/2}$ shell.

If we switch on residual interactions, the GSEs in panels (b)–(d) in Figs. 4–12 look like they retain their double valley evolutions, but their depths are largely moderated by the occupation probabilities calculated by the DBCS. Therefore, deformation positions for the minimal GSEs turn out to depend on the pairing energy types. Here the GSE evolution by the DBCS model, which is a sum of $E_{MF'} + E_{\mathrm{pair}} + E_{\mathrm{self}}$, denoted as black, blue, and green, included the np pairing as well as the nn- and pp-pairing correlations and the self-energy. We estimate them with three different cases. Panels (b) and (c) are without and with the np-pairing correlations, respectively. Panels (d) are with the enhanced np pairing and the self-energy within the DBCS scheme. Since the HFB effects turn out to be so small, we did not show them in this paper.

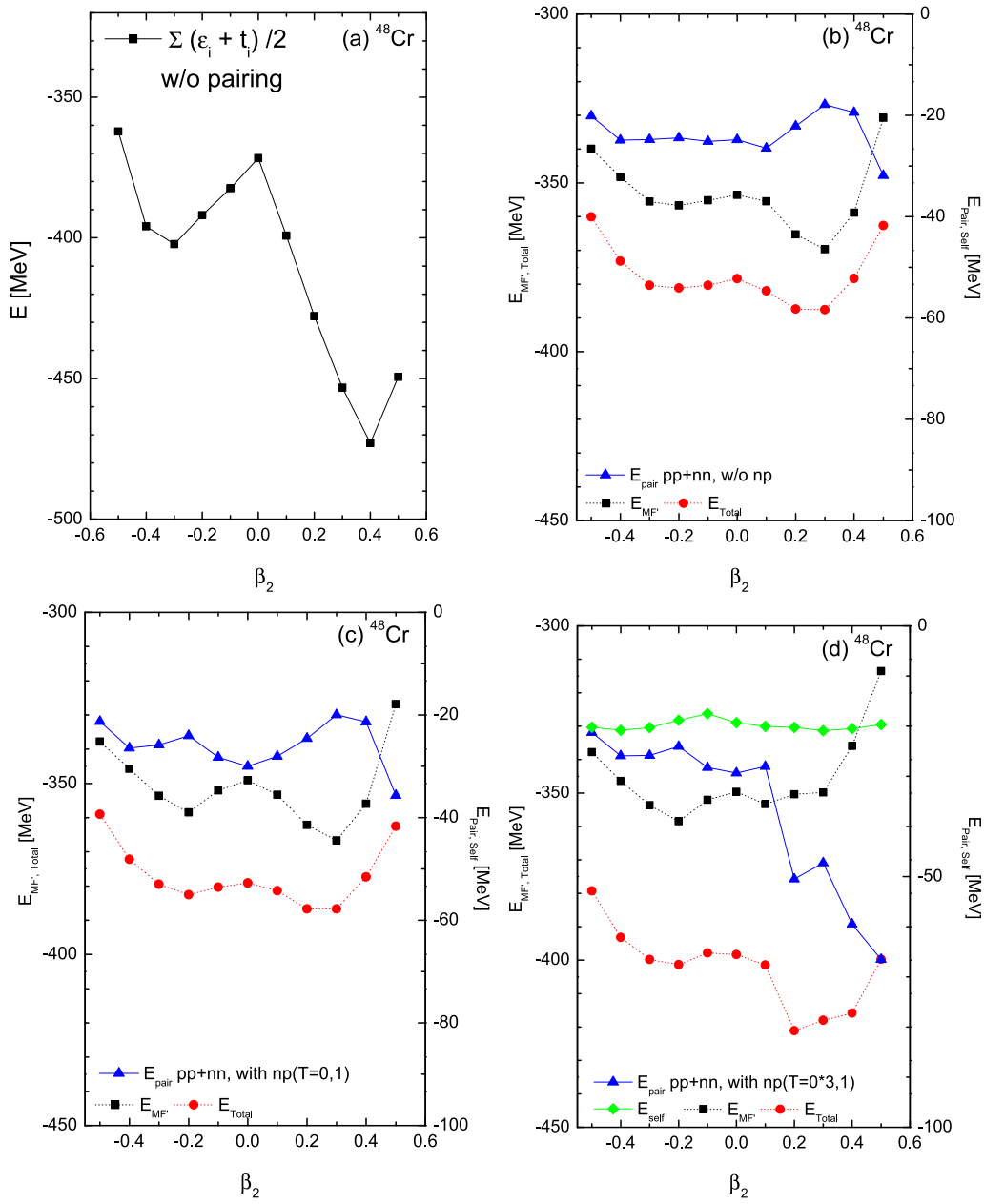

FIG. 5. The same as Fig. 4, but for ^{48}Cr.

1. ^{44}Ti and ^{48}Cr

In Fig. 4, we show GSEs by the simple shell-filling model for ^{44}Ti in Fig. 4(a). $E_{MF'}$ (black squares) in Figs. 4(b)–4(d) is the mean-field energy corrected by the smearing due to the occupation probabilities v_i^2 by the DBCS approach. Pairing energies, $E_{\rm pair}$, are denoted as blue triangles. $E_{\rm MF'}$ in Fig. 4(b) shows two valleys similarly to that by the simple shell-filling model in Fig, 4(b). This means that the like-pairing energy does not affect seriously the GSE evolution although it is largely moderated. An interesting point is that the evolution of the pairing energy in Fig. 4(b) also reflects the shell structure of Fig. 2; small shell gaps at both oblate and prolate sides near the Fermi energy. Even if the np pairing is taken into account, the pairing energy in Fig. 4(c) retains the valley around $\beta_2 \sim 0.2$ region.

Final GSEs, which are given as $E_{\rm Total} = E_{\rm pair} + E_{\rm MF'} + E_{\rm self}$, are presented as red circles in Fig. 4(d). One point to notice here is regarding a role of the enhanced $T = 0$ channel of the np-pairing correlations. We use the strong $T = 0$ contribution, enhanced about 3 times as large. It gives more bound prolate ground state compared to Fig. 4(c). That is, the enhanced $T = 0$ pairing affects more or less the shape evolution of ^{44}Ti.

Results for ^{48}Cr in Fig. 5 are not so much different from those for ^{44}Ti. Double valleys in the mean field still remain even with the DBCS smearing as shown in Fig. 5(b). These pairing correlations still make the nucleus prolate. Both strong bound features in the double valley come from the open-shell property in the $|\beta_2| \simeq 0.2$ region as shown in Fig. 2 reflected in the zigzag pattern in Fig. 5(a). Another point is that the

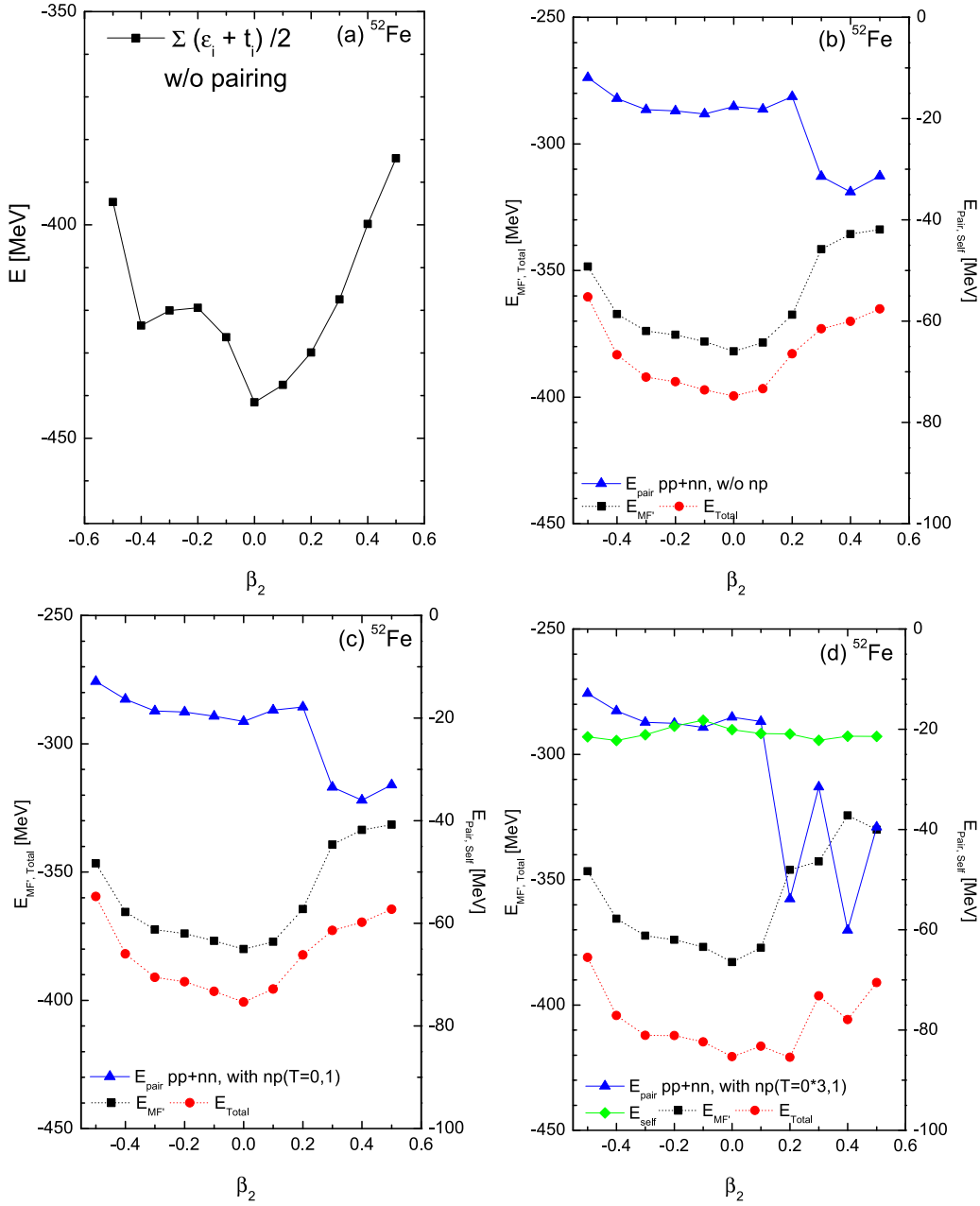

FIG. 6. The same as Fig. 4, but for ^{52}Fe.

prolate deformation of ^{48}Cr was not changed by the np-pairing correlations. However, the enhanced np-pairing correlations in Fig. 5(d) make the valley salient compared to Fig. 5(c). That is, the enhanced np pairing strongly leads the nucleus to a prolate shape.

2. ^{52}Fe and ^{64}Ge

Results by $E_{MF'}$ in Figs. 6(b) and 7(b) suggest a spherical shape for ^{52}Fe and an oblate deformation for ^{64}Ge. Even the np pairing in Figs. 6(c) and 7(c) does not change the trend. However, the enhanced np pairing for ^{52}Fe induces the stronger $E_{\rm pair}$ in the prolate region. Thus, the $E_{\rm Total}$ can reach to prolate deformation consistent with other data or evaluations. For ^{64}Ge, the situation is a bit different from that of ^{52}Fe. $E_{MF'}$ in Figs. 6(b) and 7(b) suggests an oblate deformation shape. Even $E_{\rm pair}$ by the np pairing requires the oblate deformation. That is, the np pairing still retains the oblate shape trend. However, the enhanced np pairing is shown to lead to a prolate deformation, although the minimum energy in the prolate region is only a bit deeper than the oblate region. More detailed analysis beyond the present calculation is necessary for this nucleus.

Therefore, the enhanced $T = 0$ contribution makes the bounding more stronger due to its attractive property and leads the oblate deformation to the prolate deformation. The self-energy correction does rarely depends on the deformation

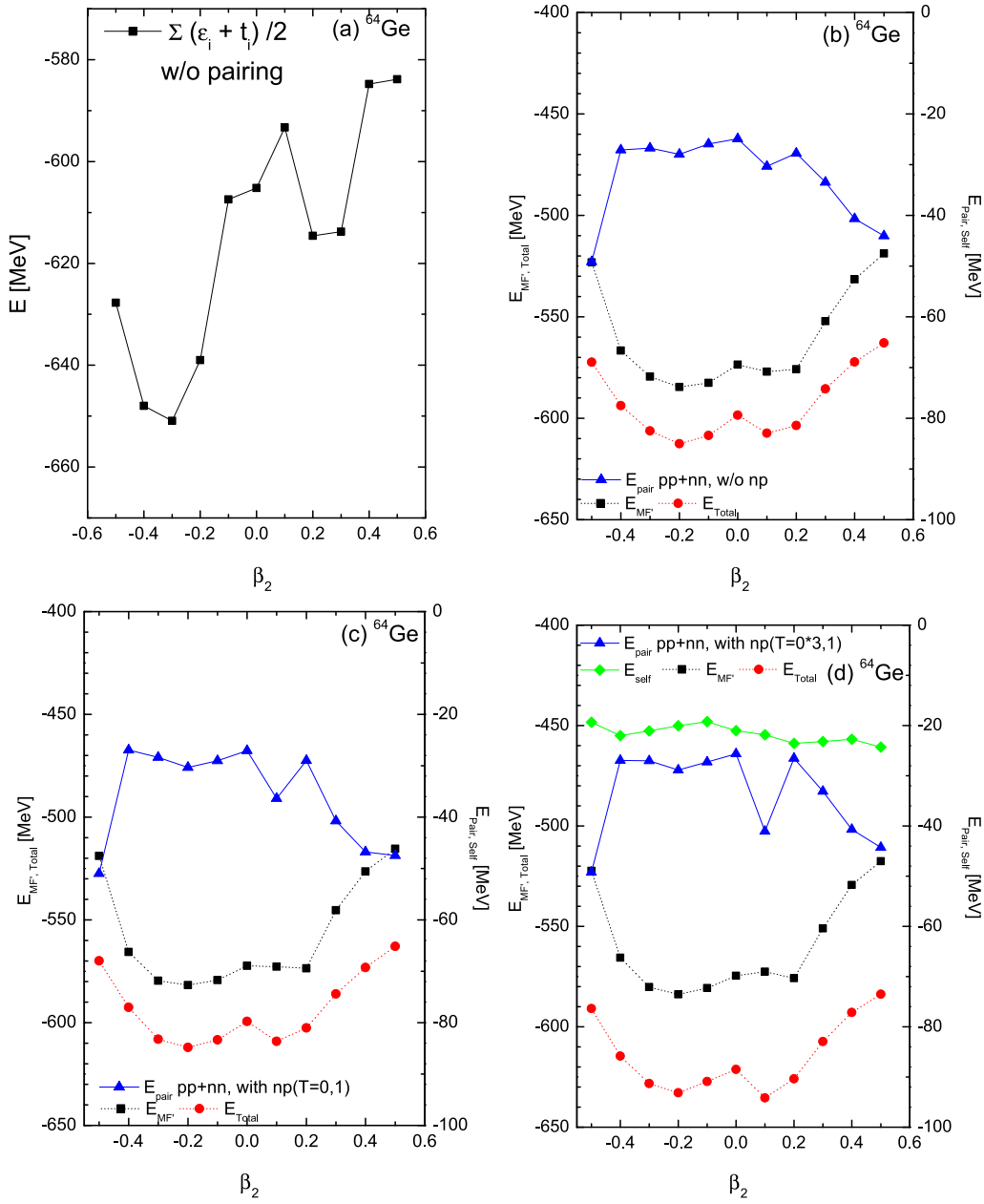

FIG. 7. The same as Fig. 4, but for ^{64}Ge.

as shown on all (d) panels. This means that the self-energy correction does not affect the evolution of total GSEs.

3. ^{68}Se, ^{72}Kr, and ^{76}Sr

Figures 8 and 9 show the shell evolution of GSEs for ^{68}Se and ^{72}Kr. Deformation signs of both nuclei in Table I are still remained to be solved, although experimental data [44,45] argued that ^{72}Kr has a strong deformation as a mixture of prolate and oblate deformations [45], and ^{68}Se shows a transitional type of γ-unstable and oblate deformations [44]. On the theoretical side, their ground states were claimed to be oblate by a constrained Hartree-Fock calculation [46] and a deformed self-consistent HF+RPA approach with density-dependent effective interaction [47].

In the present calculation, first, we note, without pairing, the oblate minimum for ^{68}Se in Fig. 8(a). This can be understood because the Nilsson model shows large energy gaps versus quadrupole deformation at $Z(=N)=34$ and 36 for oblate and prolate deformations as shown in Fig. 2. However, the energy minimum for ^{72}Kr in Fig. 9(a) has a spherical shape. The spherical minimum also comes from the SPS in Fig. 2. If we trace the $N=36$ Fermi energy line by the shell-filling model, the spherical shape would be the most stable without the pairing energy contributions even if we take into account the shell corrections by using $\frac{1}{2}\Sigma_i(\epsilon_i+t_i)$.

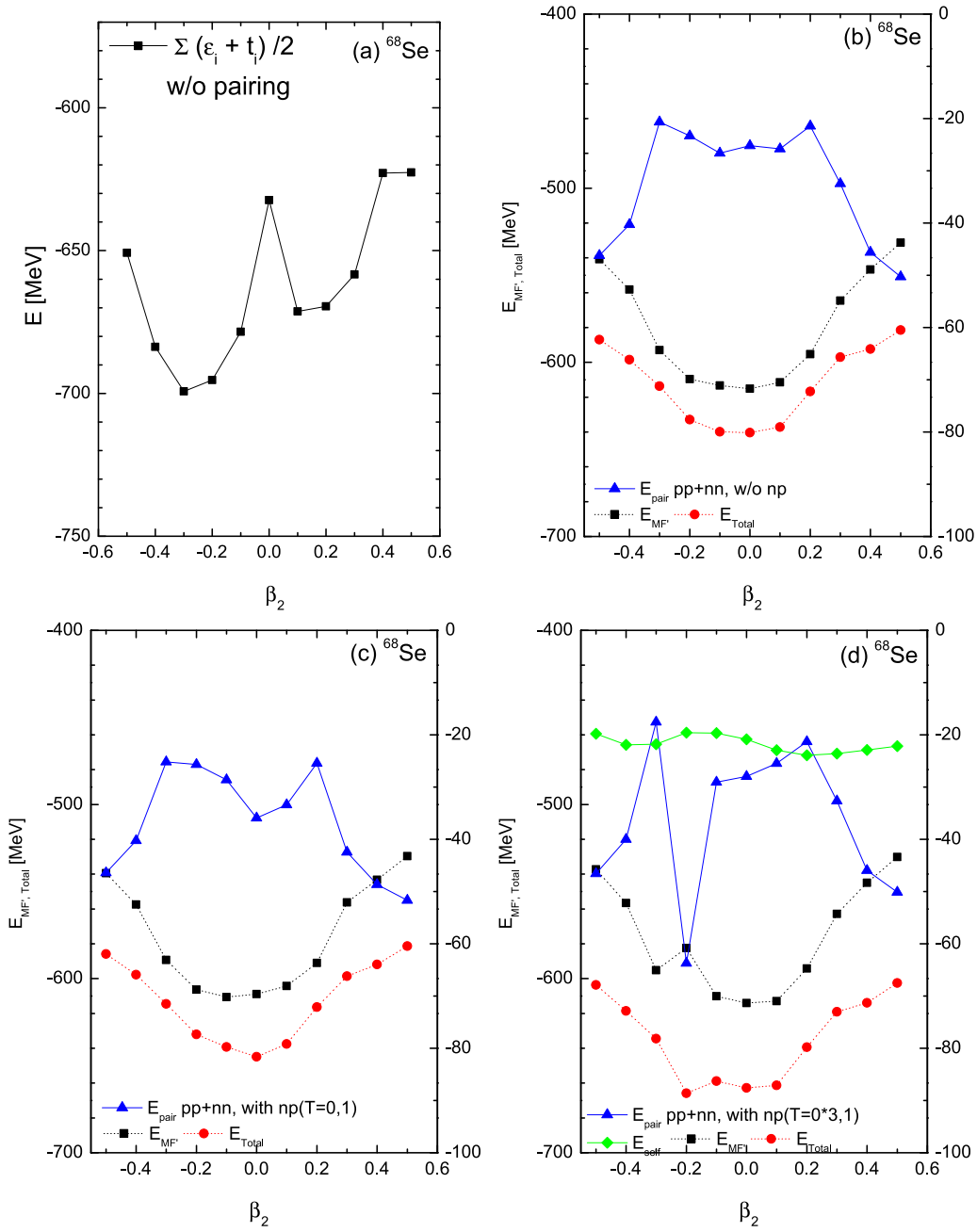

FIG. 8. The same as Fig. 4, but for ^{68}Se.

The double local minima in the mean-field theories in Figs. 8(a) and 9(a) by the simple shell-filling model are changed to have a single valley around $\beta_2 \sim 0$ region by the DBCS smearing as shown in Figs. 8(b), 9(b) and 8(c), 9(c) even with the np pairing. The unlike np-pairing correlations do not affect so much the shell evolution by the like-pairing correlations and make only the nucleus more bound. Namely, the spherical shapes of ^{68}Se and ^{72}Kr were not changed by the unlike-pairing correlations. However, the enhanced $T = 0$ pairing shifts the deformation to some oblate deformation regions as shown in Figs. 8(d) and 9(d).

Contrary to ^{52}Fe and ^{64}Ge, mean-field energies $E_{MF'}$ of ^{68}Se and ^{72}Kr show a parabola-type behavior with the deformation due to the pairing energy as shown in Figs. 8 and 9. However, the enhanced $T = 0$ pairing correlations make it oblate deformation as shown in Figs. 8(d) and 9(d). This behavior is quite different from the above two nuclei, ^{52}Fe and ^{64}Ge. It is an interesting result because ^{52}Fe and ^{64}Ge do not evolve to the oblate deformation even if we exploit the enhanced $T = 0$ strength.

The reason for this transition to the oblate region by the enhanced $T = 0$ pairing can be understood in Fig. 10. In this figure, one may notice interestingly different behavior of curves of the g_{np} and g^*_{np} for larger deformation $|\beta_2| > 0.3$. Namely, both the g_{np} and g^*_{np} keep almost the same value in the region $|\beta_2| < 0.2$ region, but g^*_{np} becomes smaller in both

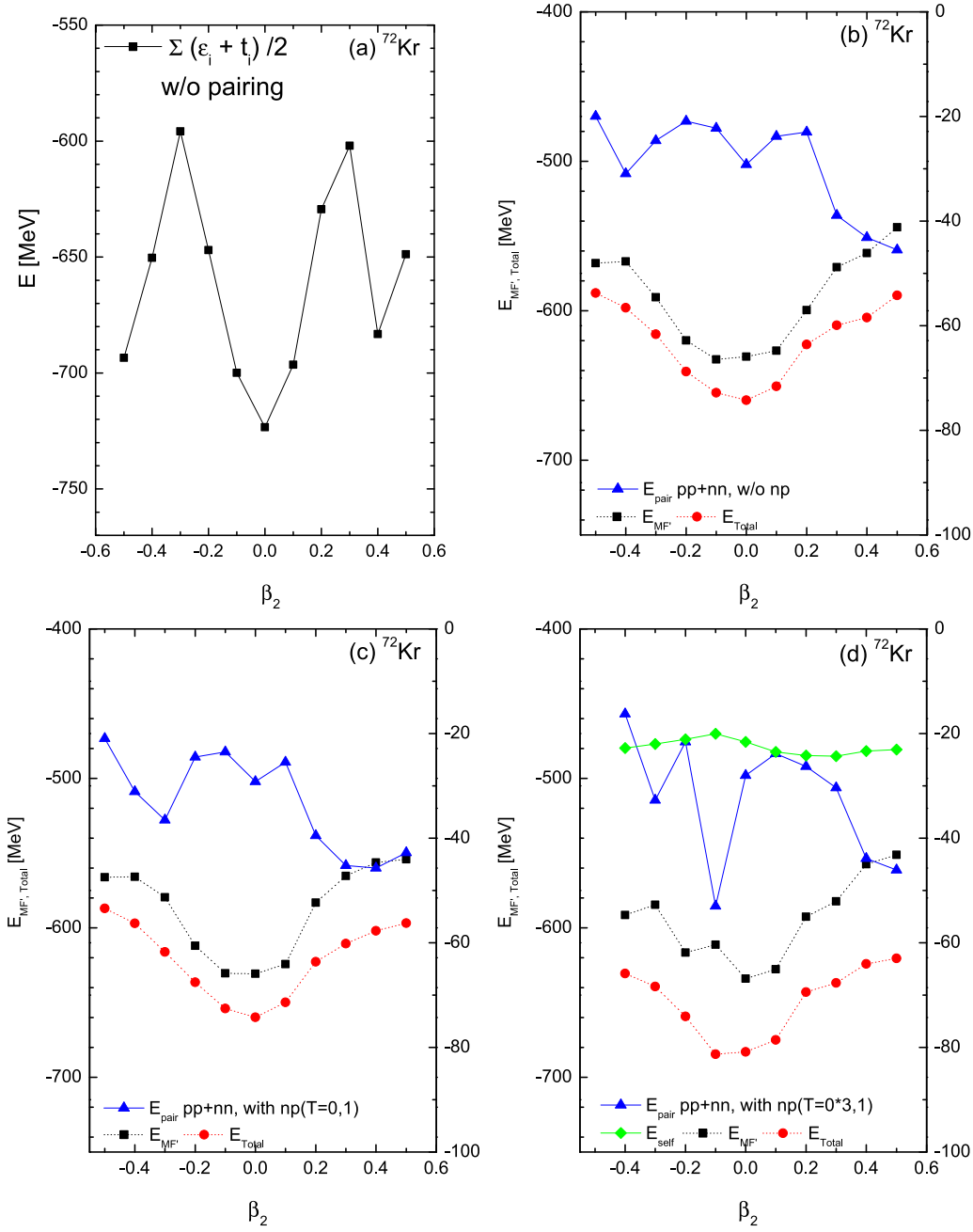

FIG. 9. The same as Fig. 4, but for ^{72}Kr.

the larger prolate and oblate deformation region $|\beta_2| > 0.3$. This is due to the effect of the $T = 0$ pairing condensation, which makes additional $T = 0$ correlations to the gap energy usually dominated by the $T = 1$ np contributions. These results suggest a manifestation of coexistence of two types of superconductivities ($T = 0$ and $T = 1$) in this large deformed region, similarly to the results found in sd-shell $N = Z$ nuclei [34].

More detailed discussions regarding which deformation is the most stable in these nuclei are done in Fig. 11. A sudden drop of the pairing energy of ^{68}Se [see Fig. 8(d)] in the $\beta_2 = -0.2$ region by the enhanced $T = 0$ pairing channel comes from the wider smearing of the proton and neutron Fermi surfaces at the deformation. Figure 11 shows how largely the deformation affects the smearing for ^{68}Se. For example, if we compare the smearing by the enhanced $T = 0$ pairing, black squares in Figs. 11(a) and 11(b), the smearing at $\beta_2 = -0.2$ [Fig. 11(b)] starts earlier around -30 MeV up to -5 MeV compared to the $\beta_2 = -0.1$ case [Fig. 11(a)], which can also be easily confirmed if we note the significant deviations of black squares from red circles in Fig. 11(b). The large smearing change in $\beta_2 = -0.2$ comes mainly from the two states, $9/2^+_1$ and $7/2^+_1$ states, in $0g_{9/2}$ shell and the $5/2^-_2$ state in $0f_{5/2}$ shell, whose occupation probabilities are increased by the enhanced $T = 0$ pairing due to their greater decrease of the SPS in the $\beta_2 = -0.2$ rather than $\beta_2 = -0.1$ region. Note their uphill

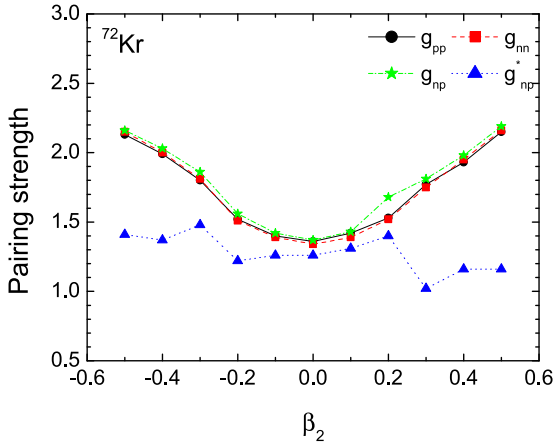

FIG. 10. Strength parameters evolution with the deformation for ^{72}Kr. Here g^{*}_{np} means the case by the enhanced $T = 0$ pairing correlations.

shapes along the prolate deformation in Fig. 2. But, for ^{72}Kr case in Fig. 9, SPS energies of the $1/2^{-}_{5}$ and $3/2^{-}_{4}$ states in $0f_{5/2}$ shell become lower with the smaller oblate deformation, which leads the minimum to the $\beta_2 = -0.1$ region rather than $\beta_2 = -0.2$ region. Interestingly, these oblate deformations in ^{68}Se and ^{72}Kr due to the enhanced $T = 0$ pairing are in contrast with the prolate deformation in ^{44}Ti, ^{48}Cr, ^{52}Fe, and ^{64}Ge whose pairing energy become deeper in the prolate region by the enhanced $T = 0$ pairing. Evidently this results from the shell evolution of the states in $0f_{5/2}$ and $0g_{9/2}$ shells.

Figure 12 presents the results for ^{76}Sr, which nucleus is reported to be largely prolate deformed [48–50], contrary to the oblate deformed nuclei, ^{68}Se and ^{72}Kr. However, mean-field energy with the $nn + pp + np$-pairing correlations is minimized at the spherical shape similarly to ^{68}Se and ^{72}Kr. However, although the pairing energy itself is minimized at the oblate region $\beta_2 = -0.3$ likewise ^{68}Se and ^{72}Kr, the enhanced np pairing shifts the minimum energy position to the prolate region due to the prolate minimum in the mean field corrected by the DBCS. Therefore, this nucleus could also give a clue for the IS condensation in the pf-shell $N = Z$ nuclei. However, this deformation for ^{76}Sr is smaller rather than the deformation reported in Refs. [48–50]. It may come from the limit of our present approach as addressed in the following.

Finally, the following point should be noted for more definite conclusions. All of our results are obtained by the DBCS (or DHFB), which keeps correct average particle numbers, but does not guarantee exact particle numbers in the ground state because of particle number fluctuations. The Lipkin-Nogami (LN) BCS theory is known as an approach to cure this problem. Actually, Ref. [38] calculated like-pairing gaps using various pairing models and compared the LN results to the BCS theory, in which the results by both the LN and the BCS theory show a similar minimum deformation in the shell evolution of the ground state of ^{48}Cr, but pairing gaps become more or less moderated by the LN method. For the exact particle number conservation, we had to rely on the number projected BCS (PBCS) theory [39], which needed a much more time-consuming process. A few modern calculations by the PBCS are being developed by many papers [40–42], but still applied only to some simple model cases.

IV. SUMMARY AND CONCLUSION

In this work, we studied evolution of single-particle state (SPS) energies for $N = Z$ nuclei in pf shell by exploiting a deformed Woods-Saxon potential. By taking the SPS as a mean-field energy, we calculated ground-state energies of the nuclei by including the pairing interactions of like- and unlike-pairing correlations in the deformed BCS (or HFB) framework. The pairing correlations turn out to be sensitive on the deformation parameter β_2 and evolve Fermi energies ϵ_f along the deformation.

The pairing effects bound the nucleus more strongly, but do change the evolution of ground-state energies so much. The np pairing also contributes to making more bound nuclei. In particular, the enhanced $T = 0$ pairing correlations, which played vital roles to determine nuclear deformations of sd-shell nuclei [34], also affect significantly the pf-shell nuclear deformation. Specifically, the oblate deformations of ^{68}Se and ^{72}Kr and prolate deformations of ^{52}Fe, ^{64}Ge, and ^{76}Sr would not be explained without the enhanced $T = 0$ pairing correlations. Finally, the HFB approach including the pairings among different states does not give any discernible effects

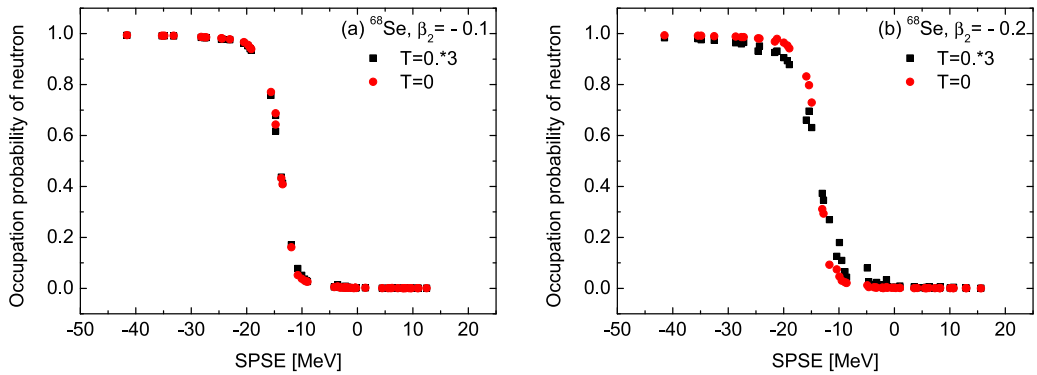

FIG. 11. Comparison of the occupation probabilities of neutrons by the enhanced $T = 0$ pairing for ^{68}Se with (a) $\beta_2 = -0.1$ and (b) -0.2. Black squares are for the enhanced $T = 0$ case.

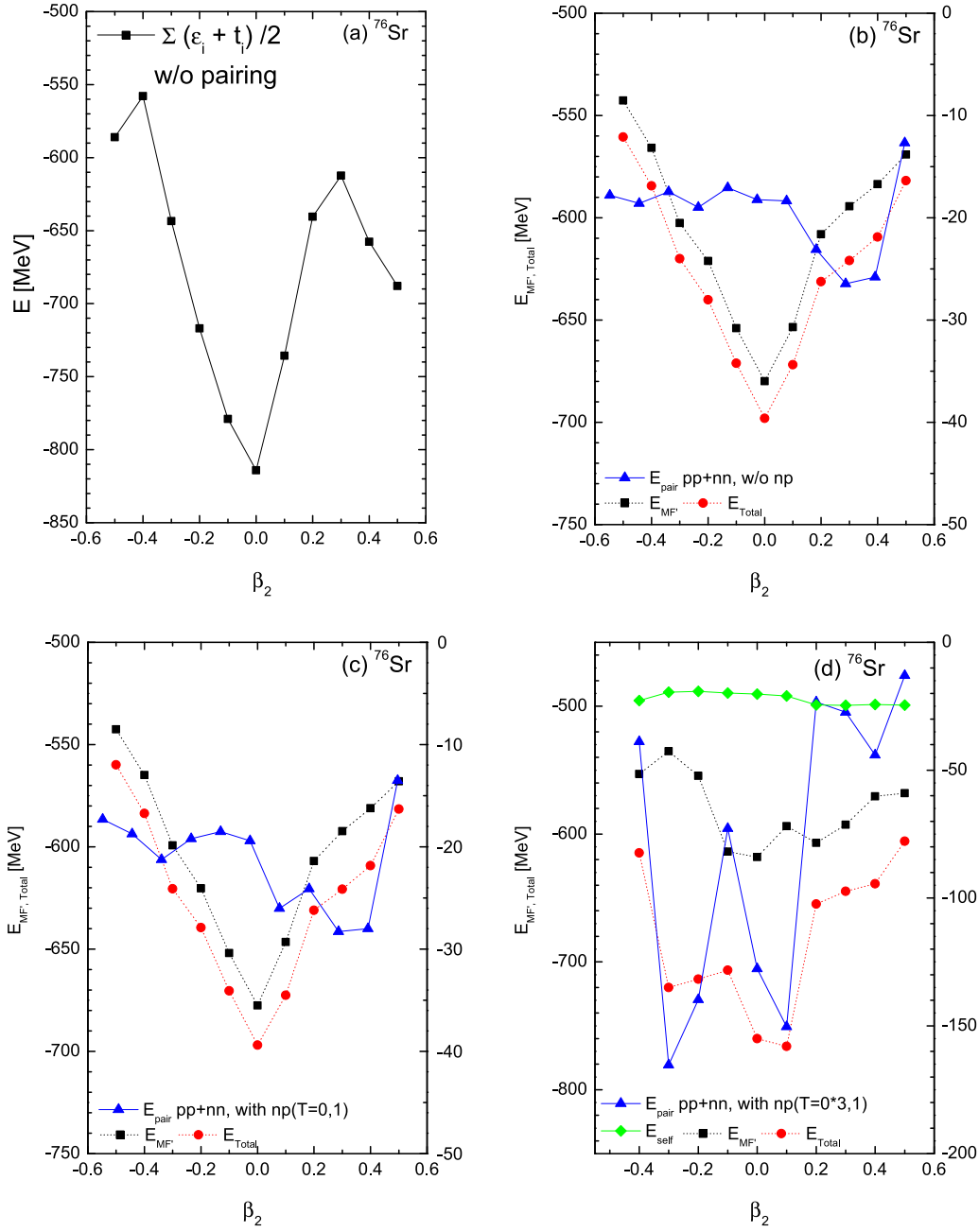

FIG. 12. The same as Fig. 4, but for ^{76}Sr.

on the nuclear structure, but contribute to more reasonable renormalization of the strength parameter for the nuclear interaction inside nuclei. Also the nucleon self-energy due to the pairing correlations rarely affect the shape evolution because its effect turns out to be nearly independent of the deformation.

In conclusion, evolution of ground-state energies by a simple shell model is mainly determined by the evolution of the outermost shell. However, the pairing interactions change significantly the evolution. The pairing energy itself is not large enough to change the evolution, but make the nuclei more bound by changing the Fermi energies (or chemical potentials), which affect the evolution seriously. In particular, the enhanced isoscalar pairing interaction is shown to play an important role in shape deformations even in the pf-shell $N = Z$ nuclei such as ^{68}Se, ^{72}Kr, and ^{76}Sr. This means that the IS condensation by the enhanced $T = 0$ pairing may happen not only in sd shell, but also in pf-shell nuclei. In addition, the pairing interactions among different states are shown to rarely affect nuclear structures compared to the conventional like pairing by the BCS approach. However, for more definite conclusion of the pairing and the deformation, one needs to develop more realistic projected DBCS or DHFB theory to retain exact particle number conservation. This work will be

extended to fpg-shell nuclei, where more interesting deformed structure, such as coexistence of oblate and prolate shapes, are reported recently [46]. Also, detailed calculations for the Gamow-Teller strength distributions [48] are in progress in the deformed QRPA formalism based on the DBCS approach in the present paper.

ACKNOWLEDGMENTS

This work was supported by the National Research Foundation of Korea (Grants No. NRF-2015R1D1A4A01020477, No. NRF-2015K2A9A1A06046598, and No. NRF-2017R1E1A1A01074023).

[1] I. Hamamoto, Phys. Rev. C **93**, 054328 (2016).
[2] I. Hamamoto, Phys. Scripta **91**, 023004 (2016).
[3] S. G. Nilsson and I. Ragnarsson, *Shapes and Shells in Nuclear Structure* (Cambridge University Press, Cambridge, 1995).
[4] S. Cwiok *et al.*, Comput. Phys. Commun. **46**, 379 (1987).
[5] R. Noyarov, J. Phys. G **10**, 539 (1984).
[6] P. Ring, Y. K. Gambhir, and G. A. Lalazissis, Comput. Phys. Commun. **105**, 77 (1997).
[7] B. Pritychenko, M. Birch, B. Singh, and M. Horoi, At. Data Nucl. Data Tables **107**, 1 (2016).
[8] B. Pritychenko *et al.*, At. Data Nucl. Data Tables **98**, 798 (2012).
[9] G. A. Lalazissis, S. Raman, and P. Ring, At. Data Nucl. Data Tables **71**, 1 (1999).
[10] P. Moller, J. R. Nix, W. D. Myers, and W. J. Swiatecki, At. Data Nucl. Data Tables **59**, 185 (1995).
[11] M. K. Cheoun, A. Bobyk, A. Faessler, F. Šimkovic, and G. Teneva, Nucl. Phys. A **561**, 74 (1993); **564**, 329 (1993); M. K. Cheoun, A. Faessler, F. Šimkovic, G. Teneva, and A. Bobyk, *ibid.* **587**, 301 (1995).
[12] C. Frohlich, G. Martinez-Pinedo, M. Liebendorfer, F.-K. Thielemann, E. Bravo, W. R. Hix, K. Langanke, and N. T. Zinner, Phys. Rev. Lett. **96**, 142502 (2006).
[13] Yi Hua Lam, Jianjun He, Hendrik Schatz, B. Alex Brown, and Anuj Parikh, PoS **INPC2016**, 144 (2017).
[14] J.-U. Nabi and M. Boeyuekata, Nucl. Phys. A **947**, 182 (2016).
[15] H. T. Chen and A. Goswami, Phys. Lett. B **24**, 257 (1967).
[16] H. H. Wolter, A. Faessler, and P. U. Sauer, Phys. Lett. B **31**, 516 (1970).
[17] A. L. Goodman, Phys. Rev. C **58**, R3051(R) (1998).
[18] F. Šimkovic, Ch. C. Moustakidis, L. Pacearescu, and A. Faessler, Phys. Rev. C **68**, 054319 (2003).
[19] J. Engel, S. Pittel, M. Stoitsov, P. Vogel, and J. Dukelsky, Phys. Rev. C **55**, 1781 (1997).
[20] O. Civitarese, M. Reboiro, and P. Vogel, Phys. Rev. C **56**, 1840 (1997).
[21] J. Engel, K. Langanke, and P. Vogel, Phys. Lett. B **389**, 211 (1996).
[22] W. Satula and R. Wyss, Phys. Lett. B **393**, 1 (1997).
[23] A. Gezerlis, G. F. Bertsch, and Y. L. Luo, Phys. Rev. Lett. **106**, 252502 (2011).
[24] H. Matsubara, A. Tamii, H. Nakada, T. Adachi, J. Carter, M. Dozono, H. Fujita, K. Fujita, Y. Fujita, K. Hatanaka, W. Horiuchi, M. Itoh, T. Kawabata, S. Kuroita, Y. Maeda, P. Navrátil, P. von Neumann-Cosel, R. Neveling, H. Okamura, L. Popescu, I. Poltoratska, A. Richter, B. Rubio, H. Sakaguchi, S. Sakaguchi, Y. Sakemi, Y. Sasamoto, Y. Shimbara, Y. Shimizu, F. D. Smit, K. Suda, Y. Tameshige, H. Tokieda, Y. Yamada, M. Yosoi, and J. Zenihiro, Phys. Rev. Lett. **115**, 102501 (2015).
[25] E. Garrido, P. Sarriguren, E. Moya de Guerra, and P. Schuck, Phys. Rev. C **60**, 064312 (1999).
[26] E. Garrido, P. Sarriguren, E. Moya de Guerra, U. Lombardo, P. Schuck, and H. J. Schulze, Phys. Rev. C **63**, 037304 (2001).
[27] H. Sagawa, C. L. Bai, and G. Colo, Phys. Scr. **91**, 083011 (2016).
[28] S. Frauendorf and A. O. Miacchiavelli, Prog. Part. and Nucl. Phys. **78**, 24 (2014).
[29] H. Sagawa, T. Suzuki, and M. Sasano, Phys. Rev. C **94**, 041303(R) (2016).
[30] C. Qi and R. Wyss, Phys. Scr. **91**, 013009 (2016).
[31] B. Bulthuis and A. Gezerlis, Phys. Rev. C **93**, 014312 (2016).
[32] G. Pantis, F. Šimkovic, J. D. Vergados, and A. Faessler, Phys. Rev. C **53**, 695 (1996).
[33] M. K. Cheoun, A. Faessler, F. Šimkovic, and G. Teneva, Prog. Part. Nucl. Phys. **32**, 315 (1994).
[34] E. Ha, M.-K. Cheoun, and H. Sagawa, Phys. Rev. C **97**, 024320 (2018).
[35] E. Ha, M.-K. Cheoun, and F. Šimkovic, Phys. Rev. C **92**, 044315 (2015).
[36] E. Ha and M.-K. Cheoun, Phys. Rev. C **88**, 017603 (2013).
[37] E. Ha and M.-K. Cheoun, Phys. Rev. C **94**, 054320 (2016).
[38] P.-G. Reinhard, W. Nazarewicz, M. Bender, and J. A. Maruhn, Phys. Rev. C **53**, 2776 (1996).
[39] G. Teneva, F. Simkovic, A. Bobyk, M. K. Cheoun, A. Faessler, and S. B. Khadkikar, Nucl. Phys. A **586**, 249 (1995); Prog. Part. Nucl. Phys. **32**, 329 (1994).
[40] L. Y. Jia, Nucl. Phys. A **941**, 293 (2015).
[41] D. Gambacurta and D. Lacroix, J. Phys. Conf. Ser. **580**, 012504 (2015).
[42] J. Dukelsky, S. Pittel, and C. Esebbag, Phys. Rev. C **93**, 034313 (2016).
[43] E. Ha and M.-K. Cheoun, Euro. Phys. J. A **53**, 26 (2017).
[44] A. Obertelli, T. Baugher, D. Bazin, J.-P. Delaroche, F. Flavigny, A. Gade, M. Girod, T. Glasmacher, A. Goergen, G. F. Grinyer, W. Korten, J. Ljungvall, S. McDaniel, A. Ratkiewicz, B. Sulignano, and D. Weisshaar, Phys. Rev. C **80**, 031304(R) (2009).
[45] J. A. Briz, E. Nácher, M. J. G. Borge, A. Algora, B. Rubio, P. Dessagne, A. Maira, D. Cano-Ott, S. Courtin, D. Escrig, L. M. Fraile, W. Gelletly, A. Jungclaus, G. Le Scornet, F. Maréchal, C. Miehé, E. Poirier, A. Poves, P. Sarriguren, J. L. Taín, and O. Tengblad, Phys. Rev. C **92**, 054326 (2015).
[46] K. Kaneko, M. Hasegawa, and T. Mizusaki, Phys. Rev. C **70**, 051301(R) (2004).
[47] P. Sarriguren, E. Moya de Guerra, and A. Escuderos, Nucl. Phys. A **658**, 13 (1999).
[48] A. B. Peres-Cerdan *et al.*, Phys. Rev. C **88**, 014324 (2013).
[49] E. Nácher, A. Algora, B. Rubio, J. L. Taín, D. Cano-Ott, S. Courtin, P. Dessagne, F. Maréchal, C. Miehé, E. Poirier, M. J. G. Borge, D. Escrig, A. Jungclaus, P. Sarriguren, O. Tengblad, W. Gelletly, L. M. Fraile, and G. Le Scornet, Phys. Rev. Lett. **92**, 232501 (2004).
[50] A. Lemasson, H. Iwasaki, C. Morse, D. Bazin, T. Baugher, J. S. Berryman, A. Dewald, C. Fransen, A. Gade, S. McDaniel, A. Nichols, A. Ratkiewicz, S. Stroberg, P. Voss, R. Wadsworth, D. Weisshaar, K. Wimmer, and R. Winkler, Phys. Rev. C **85**, 041303(R) (2012).